NORSAR

ROYAL NORWEGIAN COUNCIL FOR SCIENTIFIC AND INDUSTRIAL RESEARCH

Scientific Report No. 2-84/85

SEMIANNUAL TECHNICAL SUMMARY

1 October 1984 – 31 March 1985

L. B. Loughran (Ed.)

Kjeller, July 1985

VII.10.1 Crustal structure in the NORSAR array siting area derived from gravity observations

The NORSAR array is sited at the outskirts of the paleo Oslo Rift/ Oslo Graben system, which is geophysically characterized by a pronounced gravity high. These data may provide details on the crustal structure in the NORSAR area as the array's seismic recordings, despite much research ingenuity, have proved to be essentially transparent to local heterogeneities due to near-vertical angles of incidence of the teleseismic waves (e.g., see Aki et al 1977; Christoffersson and Husebye, 1979; Haddon and Husebye, 1979; Troitskiy et al, 1981; and Tompson and Gubbins, 1981). Crustal profiling surveys and local earthquake recordings are not particularly helpful in this respect and the non-uniqueness inherent in refraction profiling types of surveys (no cross-sampling) remain a problem (e.g., see Cassell et al, 1983; Mereu et al, 1983).

Clearly, crustal structural details are important for an improved understanding of complexities in high quality seismic records like those now provided by the new NORESS array, and as a first step towards solving this kind of wave propagation/scattering problems we have attempted to exploit the structural information implicitly contained in the easily available Oslo Graben gravity data.

Tectonic setting and the Oslo Graben residual gravity field

The tectonic setting of the general Oslo Graben area is shown in Fig. VII.10.1 and clearly implies that its evolution has been rather complex. However, on the other hand the geophysical imprints of past orogens, etc., are not preserved indefinitely, and today the Oslo Graben gravity high appears to be the outstanding feature reflecting past taphrogenesis. The gravity data coverage of the general graben area is relatively dense, altogether more than 5300 measurements have been carried out (e.g., see Ramberg, 1976). His residual gravity field is

shown in Fig. VII.10.2, and this map formed the basis for our reinterpretation (inversion) of the gravity data pertaining to the Oslo Graben area.

For the sake of completeness it should be mentioned that Ramberg attributed the observed anomalies to intrusion of relatively dense material at the base of the crust (Moho upwarp) while Husebye et al (1978) using Parker's (1975) Ideal-Body Concept gave a mid-crust location of the intrusive body. Parker's technique is very different from standard approaches as in order to reduce the non-uniqueness inherent in gravity interpretations, information extraction is optimized with respect to either density contrast or distance to causative body.

Linear density inversion

The gravity field, being a potential field, invites ambiguity in interpretations which was duly recognized at a relatively early stage of exploration. However, techniques differ in their ability to reduce the number of plausible solutions without invoking a priori information about the heterogeneous body such as density contrasts and geological structural boundaries (outcrops). Thus, inverse methods are favored because they require a minimum number of subjective judgements on the part of the interpreter.

The physical model used (see Fig. VII.10.3) is of the 2½-D kind and consists of N block-formed prisms of 200 km extent matching the approximate length of the Oslo Graben. For the i-th prism the gravitational attraction g_{ij} at the j-th observation point is a linear function of density ρ_i, that is:

$$g_{ij}(\rho_i) = \gamma\rho_i \int_V \vec{z} \cdot r_o \frac{1}{|r-r_o|} dV = a_{ij}\rho_i \qquad (1)$$

where γ = universal gravitational constant, and the volume integral equals the geometrical weighting funtion a_{ij} relating volume of the prism and its distance from the observation point.

The theoretical gravity G_j^t at N observation points is:

$$G_j^t = F_j(\vec{\rho}) = \sum_{i=1}^{M} g_{ij}(\rho_i) \qquad j = 1,N \tag{2}$$

To estimate a density distribution, we note that by substituting the "true" density values, ρ_T, into eq. (2), we get

$$G_j^t = F_j(\vec{\rho_T}) = G_j^o \qquad j = 1,N \tag{3}$$

where G_j^o is the observed gravity at point j. Since F_j is linear in density and noting that our initial density model ρ_o is related to ρ_T by

$$\vec{\rho_T} = \vec{\rho_o} + \vec{\Delta\rho} \tag{4}$$

we achieve

$$F_j(\vec{\rho_o}+\vec{\Delta\rho}) = F_j(\vec{\rho_o}) + F_j(\vec{\Delta\rho}) = G_j^o \qquad j = 1,N \tag{5}$$

Eq. (1), (2) and (5) combine to yield

$$G_j^o \cdot F_j(\vec{\rho}_o) = F_j(\vec{\Delta\rho}) = \sum_{i=1}^{M} a_{ij}\Delta\rho_i \qquad j = 1,M \tag{6}$$

Using matrix notation,

$$\vec{\Delta G} = \vec{G}^o - \vec{G}^T = A\vec{\Delta\rho} \tag{7}$$

A least squares solution to eq. (7) for $\Delta\rho$ is obtained by solving the normalized system:

$$A^TA\ \Delta\rho = A^T\ \Delta G \tag{8}$$

where T denotes transpose. Now, A can be decomposed as:

$$A = U\ \Lambda\ V^T \tag{9}$$

Inserting this in eq. (8) and taking the generalized inverse of A^TA, the estimate of the correction vector becomes:

$$\Delta\rho = V\ \Lambda^{-1}U^T\ \Delta G = H\ \Delta G \tag{10}$$

The $\Delta\rho$ estimation procedure is strictly linear since the A-matrix remains invariant.

Important by-products of the inversion procedure are the resolution and the information density matrices, defined respectively as:

$$R = HA = V\ V^T$$

$$S = AH = U\ U^T$$

For details on techniques used for solving the eq. (7) type of linear equations, reference is made to Backus and Gilbert (1968). We want to remark that the presence of small eigenvalues may cause the solution to oscillate markedly, so a lower cutoff value has to be selected. In practice, this was achieved by retaining the variance of the parameter estimate relatively small without sacrificing too much of the resolution which amounts to eliminating the influence of short wavelength noise in the data. Added flexibility in using the above inversion scheme is often desired as the initial systems of prisms (or blocks) may at a later stage in the analysis prove to be somewhat awkward. For example, it may be desirable to reduce the number of unknowns by merging prisms, or to build in a priori geological information about the likely shape of the anomalous body. Christoffersson and Husebye (1979) have demonstrated a simple scheme for incorporating such modifications without completely restructuring the A-matrix. To do so we introduce a vector θ of "free" parameters which are related to the original parameter vector via a matrix T, that is:

$$\Delta\rho = T\,\theta \qquad (11)$$

For the general case, eq. (7) and eq. (11) are to be combined:

$$\Delta G = A\,T\,\Delta\theta$$

Details on estimating resolution, standard errors, etc., for the original variables using the eq. (11) transformation can be found in Husebye and Hovland (1982).

Gravity inversion results

All the 8 residual gravity anomaly profiles (III to X) shown in Fig. VII.10.2 have been analyzed using the inversion scheme outlined in the previous section. For illustrative purposes we only display results for 3 of the profiles (Figs. VII.10.3-5), namely, III, VI and IX, as these profiles are representative of the northern, central and southern segments of the Oslo Graben. As regards practical details of

the inversion analysis like initial and final numbers of prisms used, number of eigenvalues ignored in thesolution, etc., this information is included in the respective figure captions. Furthermore, similar results and details for the other profiles can be found in Wessel (1984).

The two striking features characteristic of all profiles are: i) the small density contrast resolved and ii) the depth to the causative body. No higher value than 0.06 cm g^{-3} for the anomalous body wave were encountered during the analysis, while the corresponding excess masses are concentrated in the depth interval 15 to 20 km. The only exception here is profile III where significant excess masses are found down to 25 km. The size of the anomalous body gradually increases southward implying a widening of the graben in that direction as indicated by the surface geology as well. Furthermore, the very small discrepancies between observed and calculated gravity are reflected in low relative RMS-values of the order of 0.05 mgal.

Very recently Kibsgaard (1985) has studied fault mechanisms of small earthquakes in the northern part of the Oslo Graben (close to profile III). The very interesting feature here is that foci positions appear to be located on the flanks of the anomalous body derived from the gravity study (see Fig. VII.10.6). A tenative, physical explanation here is as follows; the primary lithosphere stress field in Fennoscandia is caused by ridge push forces originating in the Norwegian Sea (e.g., see Husebye et al, 1978) whose orientation in the graben area coincide with the compression axis reported by Kibsgaard in his study. The interaction of this field with loading stresses caused by the "heavy" intrusive body in the graben give rise to stress amplifications being largest on the lower periphery of the body and ultimately becoming causative of the majority of local earthquakes observed.

Extensive details on the gravity inversion investigation reported here, including hypotheses on Oslo Graben taphrogenesis, can be found in Wessel (1984) and Wessel and Husebye (1985).

Concluding remarks

The crustal structure model presented here and derived primarily on the basis of gravity observations is to our knowledge the most detailed ever presented for the NORSAR array siting area. Important, work is already under way to compute the "seismic responses" of these structures on crustal travelling waves. Part of the motivations for undertaking such work is that preliminary 3-comp. seismogram analysis results clearly demonstrate a consistent migration off azimuth of later arriving phases.

There is also another aspect of the Oslo Graben results, namely, the underlying dynamic mechanisms causing the formation of the relatively dense body in the central crust. To improve our ability to handle this kind of problems, a cooperative research venture with Professor H.-J. Neugebauer, Clausthal, FRG, is in the planning stages. Tangible results here so far are a simplified modelling experiment with magma intrusion in the crust as demonstrated in Fig. VII.10.7 and conducted by Dr. Neugebauer.

E.S. Husebye
P. Wessel, now at LDGO,
Columbia University

References

Aki, K., A. Christoffersson, and E.S. Husebye, Determination of the three dimensional structure of the lithosphere, J. Geophys. Res., 82, 277-296, 1977.

Backus, G., and F. Gilbert, The resolving power of gross earth data, Geophys. J. Roy. Astron. Soc., 16, 169-205, 1968.

Cassell, B.R., S. Mykkeltveit, R. Kanestrøm, and E.S. Husebye, A North Sea - southern Norway seismic crustal profile, Geophys. J. Roy. Astron. Soc., 72, 733-753, 1983.

Christoffersson, A., and E.S. Husebye, On 3-dimensional inversion of P-wave time residuals - Option for geological modeling, J. Geophys. Res., 84, 6168-6176, 1979.

Haddon, R.A.W., and E.S. Husebye, Joint interpretation of P-wave time and amplitude anomalies in terms of lithospheric heterogeneities, Geophys. J. Roy. Astron. Soc., 55, 19-44, 1978.

Hovland, J., E.S. Husebye, C.E. Lund, K. Åstrøm, and A. Christoffersson, A tomographic image of the S. Scandia lithosphere and asthenosphere, M/s in preparation, 1985.

Husebye, E.S., H. Bungum, J. Fyen and H. Gjøystdal, Earthquake activity in Fennoscandia between 1497 and 1975 and intraplate tectonics, Nor. Geol. Tidsskr., 58, 51-68, 1978.

Husebye, E.S., and J. Hovland, On upper mantle seismic heterogeneities beneath Fennoscandia, in: E.S. Husebye (Ed.), The structure of the lithosphere-asthenosphere in Europe and the North Atlantic, Tectonophysics, 90, 1-17, 1982.

Husebye, E.S., and I.B. Ramberg, Geophysical investigations, in: The Olso Paleorift, Nor. Geol. Unders., No. 337, Universitetsforlaget, Oslo, Norway, 1978.

Husebye, E.S., I.B. Ramberg, and P.C. England, The ideal-body concept in interpretation of Oslo Rift gravity data and their correlation with seismic observations, in: Ramberg, I.B., and E.-R. Neumann, (Eds.), Tectonics and Geophysics of Continental Rifts, NATO Advanced Study Institute Series C, 37, 313-327, 1978.

Ingate, S.F., E.S. Husebye, and A. Christoffersson, Regional arrays and optimum processing schemes, Bull. Seism. Soc. Am., 75, Aug 1985.

Kibsgaard, A., Fault mechanism studies using the SV/P ratio tecnique; practical application for earthquakes in Stiegler's Gorge, Tanzania, and in the Oslo Graben, Norway, Cand. scient. thesis, Inst. for Geophysics, Univ. of Oslo, Norway.

Parker, R.L., The theory of ideal bodies for gravity interpretation, Geophys. J. Roy. Soc. Lond., 149, 747-763, 1975.

Ramberg, I.B., Gravity interpretation of the Oslo graben and associated igneous rocks, Nor. Geol. Unders., 325, 193 pp, 1976.

Ramberg, I.B., and S.B. Smithson, Gravity interpretation of the southern Oslo Graben and adjacent Precambrian rocks, Norway, Tectonophysics, 11, 419-431, 1971.

Thomson, C.J., and D. Gubbins, Three-dimensional lithospheric modelling at NORSAR: linearity of the method and amplitude variations from the anomalies, Geophys. J. Roy. Astron. Soc., 71, 1-36, 1982.

Troitskiy, P., E.S. Husebye, and A. Nikolaev, Lithospheric studies based on holographic principles, Nature, 294, 618-623, 1981.

Wessel, P., Gravity inversion and Oslo Graben taphrogenesis, Cand. scient. thesis, Dept. of Geology, Univ. of Oslo, Oslo, Norway.

Wessel, P., and E.S. Husebye (1985): The Oslo Graben gravity high and taphrogenesis, manuscript submitted for publication.

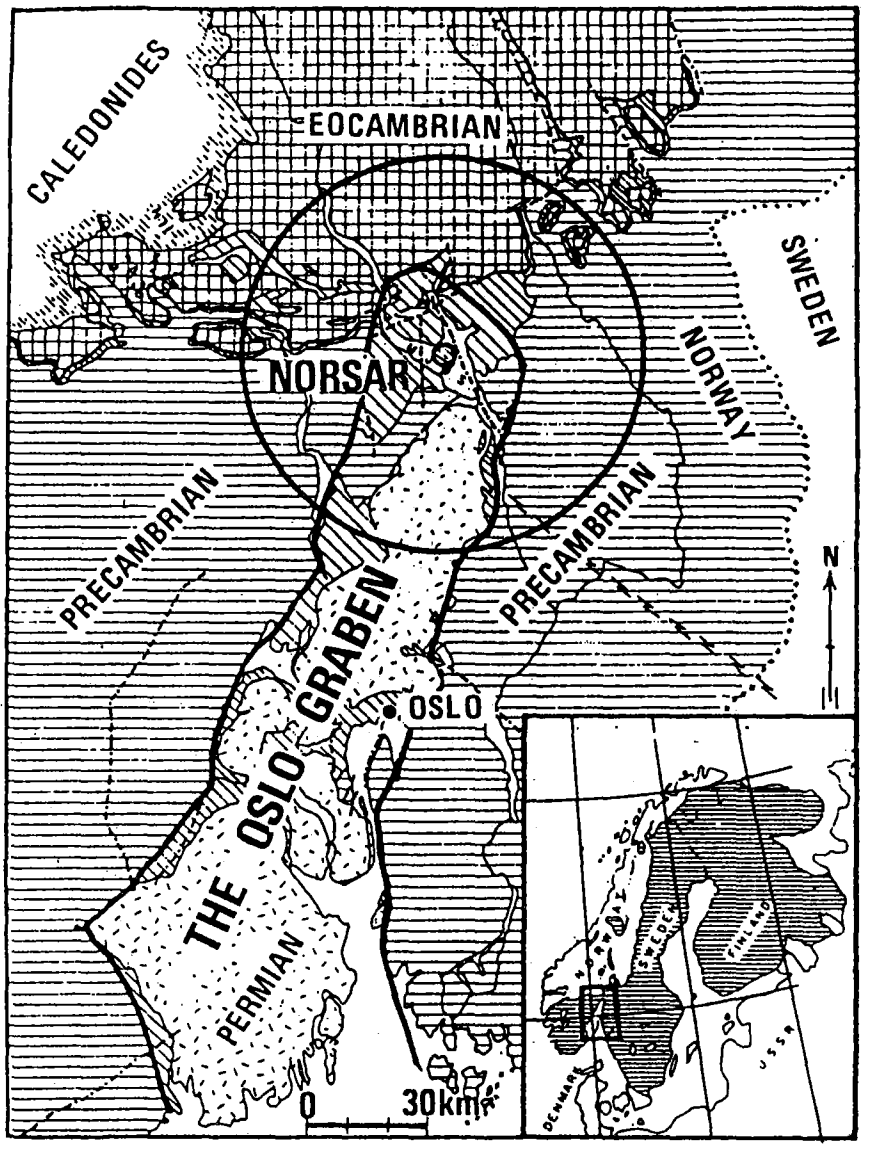

Fig. VII.10.1 The geology of the Oslo Graben and adjacent areas.

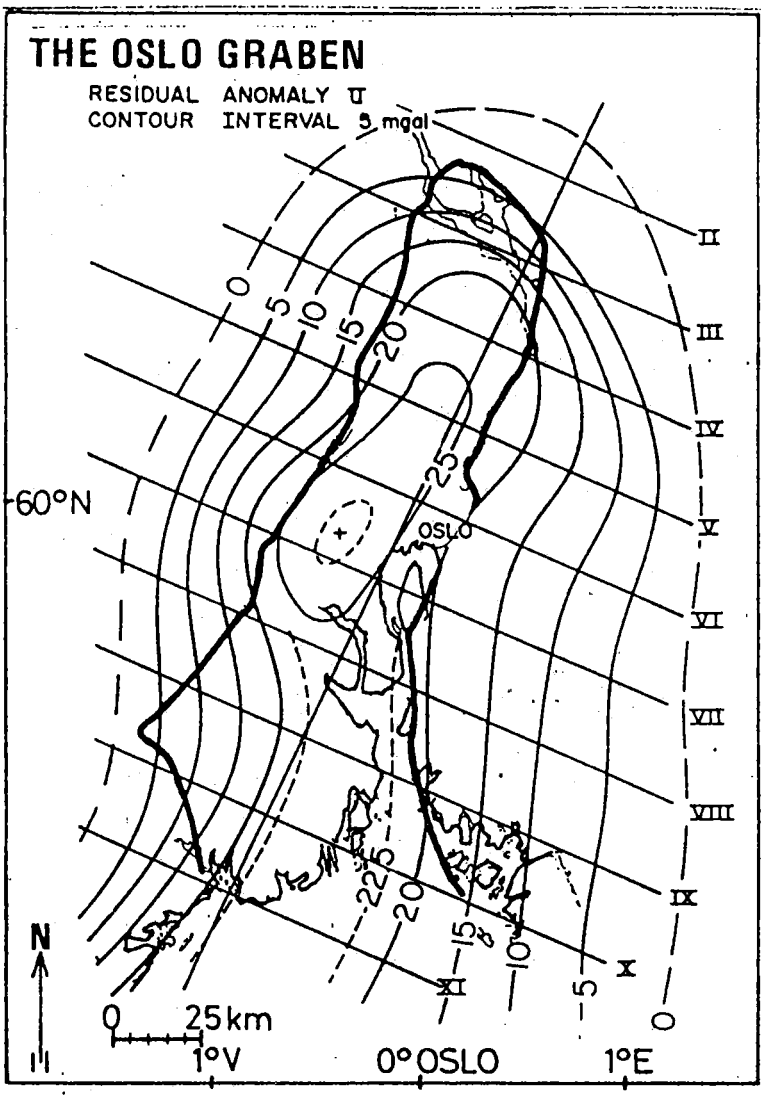

Fig. VII.10.2 The Oslo Graben residual gravity anomaly redrawn from Husebye and Ramberg (1978). The cross-sections (profiles) subjected to our block inversion analysis are indicated.

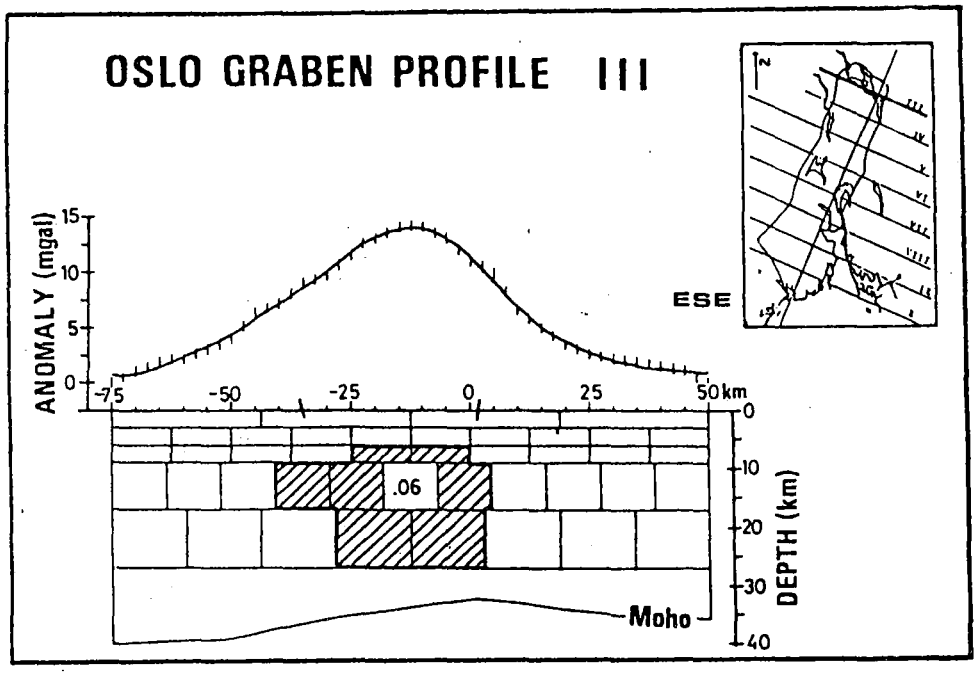

Fig. VII.10.3 Inversion results in terms of $2\frac{1}{2}$-D density contrast distribution obtained for profile III. The initial model consisted of 44 prisms, finally reduced to 35 by combining those having equal density contrast. Density contrasts for the non-hatched prisms amounted at most to $\pm$ 0.01 gcm^{-3} and this was not considered significant. Observed (vertical bars) and calculated (solid lines) gravity (RMS = 0.045) together with the Moho contours are also shown.

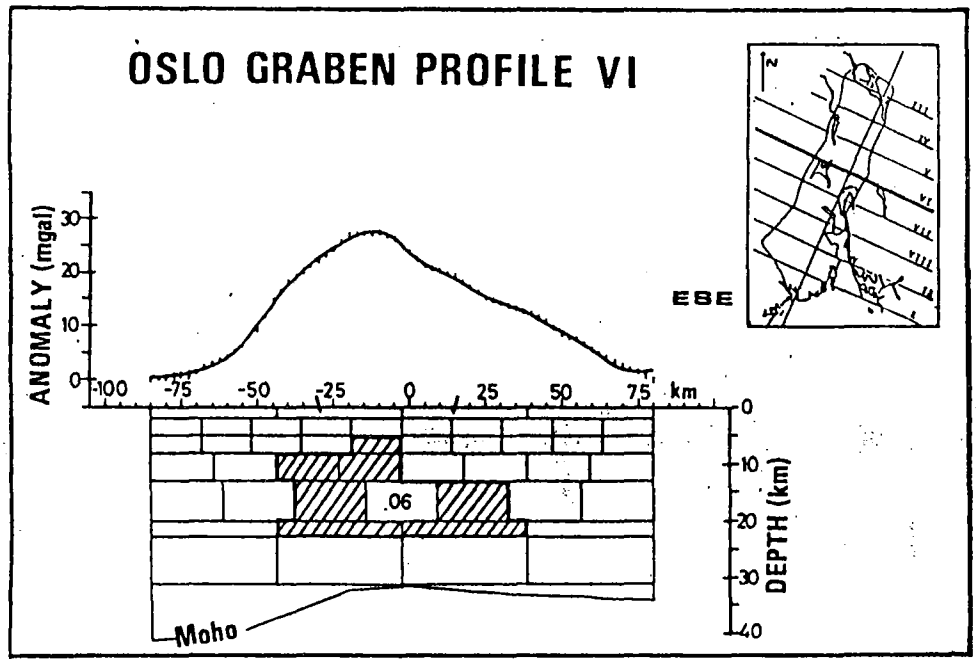

Fig. VII.10.4 Same as Fig. VII.10.3, but with initial model consisting of 48 prisms, reduced to 35. RM value = 0.050.

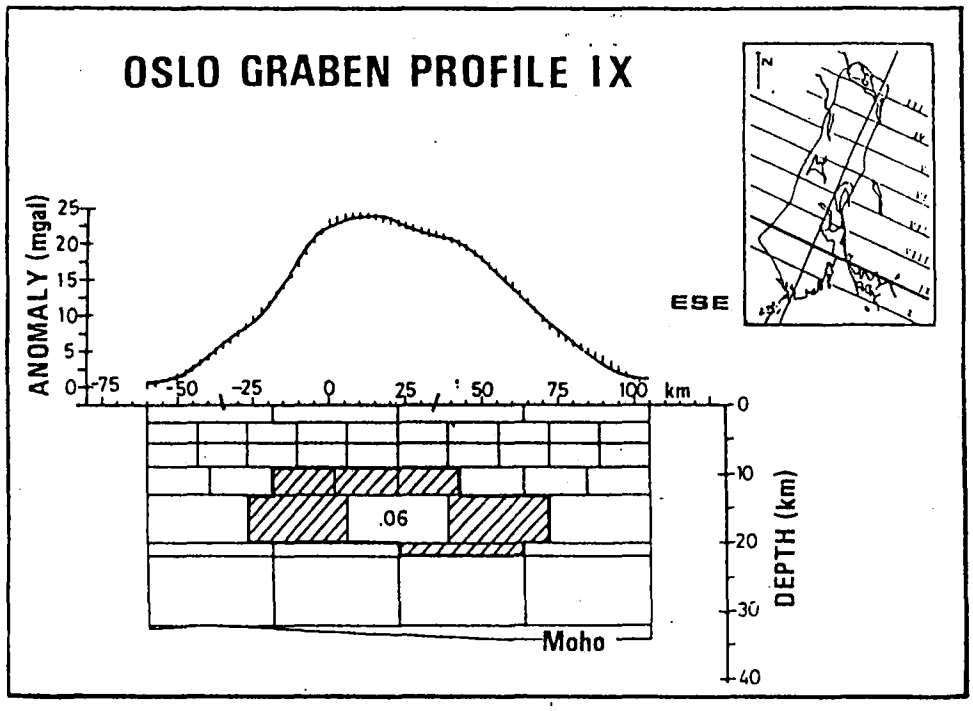

Fig. VII.10.5 Same as Fig. VII.10.4, but with initial model consisting of 46 prisms, reduced to 33. RMS value = 0.049.

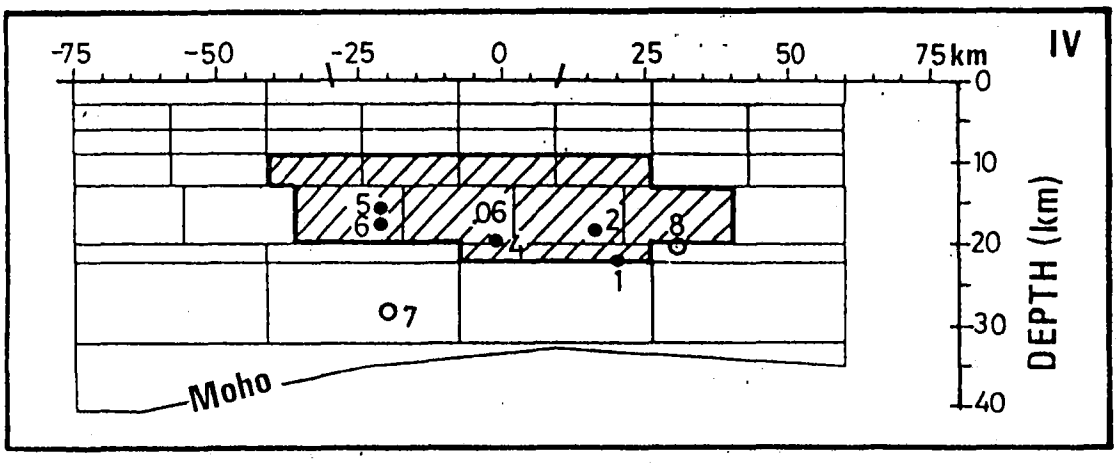

Fig. VII.10.6 Projection of hypocenters into the profile IV cross-section. It is rather remarkable that all events are located at (wrapped around) the lower part of the gravity derived anomalous body. The poorest fit is seen for event 7 whose projection into profile III gives a much better fit vs the location of that anomalous body.

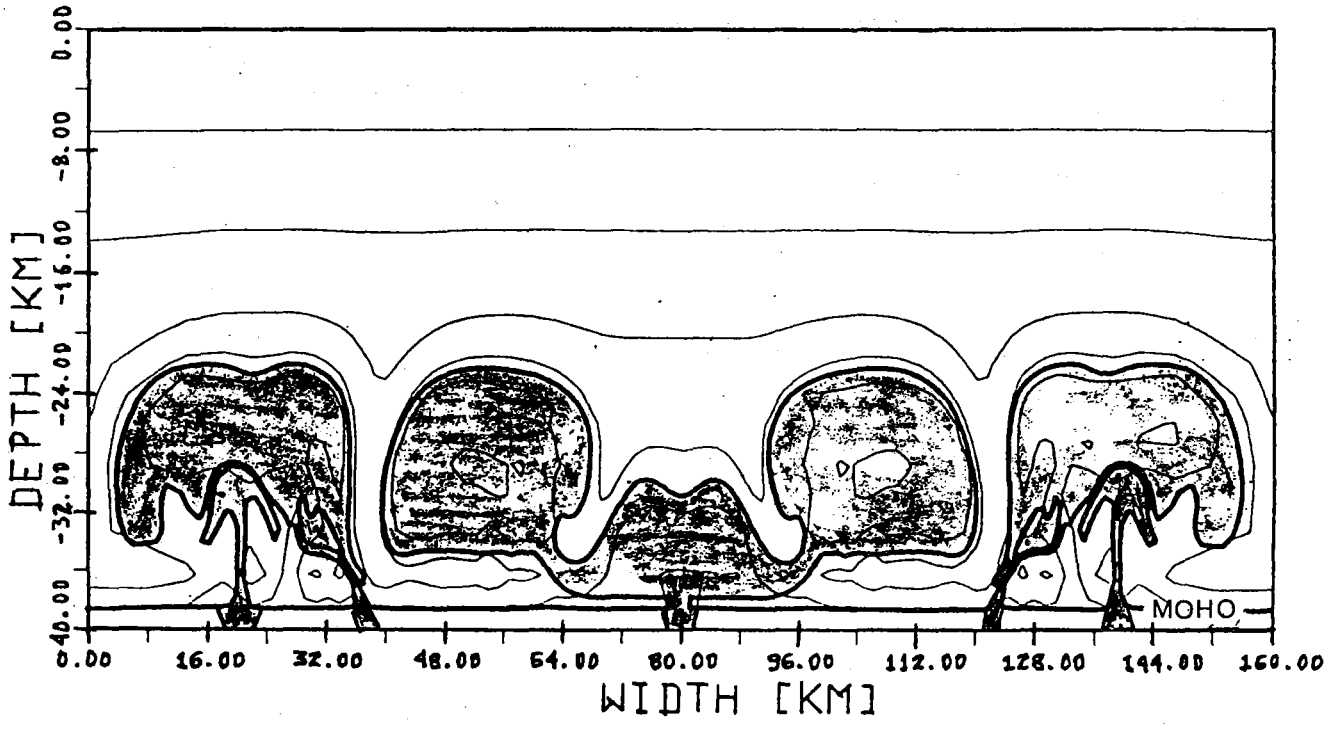

Fig. VII.10.7 Synthetic modelling of crustal intrusions for providing a deeper insight on the mechanism by which the relatively dense body in the Oslo Graben was formed. Thick lines: boundaries of intrusions; thin lines: temperature intervals of 200° (zero at surface and 1200° at bottom or Moho). Originally the model had one homogeneous intrusion, vertical viscosity contrast being 5 orders of magnitude. In the beginning the intrusion would represent a density inversion. When cooling and constracting the density contrast would be positive, but located in the lower crust, contrasting our gravity results for the Oslo Graben. All calculations here have been made by Professor H.-J. Neugebauer, Clausthal, FRG.